Sequential Learning of Visual Tracking and Mapping Using Unsupervised Deep Neural Networks

Youngji Kim and Ayoung Kim*

***Abstract*— We proposed an end-to-end deep learning-based simultaneous localization and mapping (SLAM) system following conventional visual odometry (VO) pipelines. The proposed method completes the SLAM framework by including tracking, mapping, and sequential optimization networks while training them in an unsupervised manner. Together with the camera pose and depth map, we estimated the observational uncertainty to make our system robust to noises such as dynamic objects. We evaluated our method using public indoor and outdoor datasets. The experiment demonstrated that our method works well in tracking and mapping tasks and performs comparably with other learning-based VO approaches. Notably, the proposed uncertainty modeling and sequential training yielded improved generality in a variety of environments.**

I. Introduction

Visual SLAM and VO have been extensively studied over the past decades, producing mature solutions such as [1], [2], [3], [4]. In these seminal works, carefully designed models for robust tracking and mapping were proposed. Although yielding successful results, model-based approaches still have limitations on general usage due to the sophisticated parameter tuning procedures. The ability to automatically adapt the model to new environments is still missing.

In the recent development of deep learning approaches to SLAM, structure-from-motion (SFM) problems revealed an alternative and promising solution to this issue. Among them, deep learning-based VO, which replaces the entire VO module with deep networks, has drawn attention in recent years. End-to-end learning-based VO eliminates the need for design parameters as the network directly involves with them. The sophisticated model design is no longer required; instead, motions and structures are learned from the data. Once trained with abundant data, the network is featured as a generalized model that can be applied to diverse scenes.

However, none of the recent learning-based VOs strikingly outperform model-based approaches especially in terms of accuracy, robustness, and run-time performance. One of the reasons is that existing deep VOs omit some critical procedures conducted by the conventional approach. For instance, most deep VOs are concerned only with tracking even the simultaneous consideration of mapping and local bundle adjustment (BA) is crucial for the model-based approaches. Secondly, despite the conventional model-based approach's focus on error modeling and reliable rejection techniques via uncertainty incorporation, only few [5], [6], [7] started to consider the uncertainty in deep learning approaches.

Y. Kim and A. Kim are with the Department of Civil and Environmental Engineering, KAIST, Daejeon, S. Korea [youngjikim, ayoungk]@kaist.ac.kr

This work is supported by a grant from the Korea MOTIE (No.10051867).

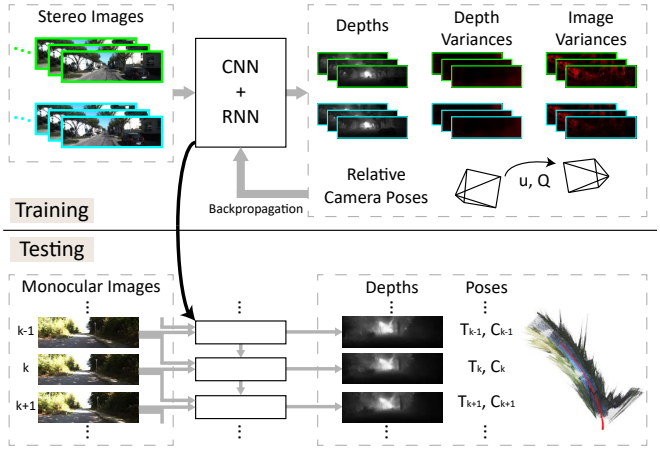

Fig. 1: Overview of the proposed system. The upper side of this figure shows the training process. With a minimal supervision, the networks are trained via minimizing a loss computed from the input stereo images and the output pose, depth and variances. In the testing phase, depth and pose are predicted from the monocular image streams sequentially inserted to the networks.

We proposed a novel learning-based VO for the sake of reproducing properties of the model-based VO as shown in Fig. 1. We tackle the complete end-to-end implementation by introducing a Convolutional Neural Network (CNN) and a Recurrent Neural Network (RNN). Just as in the conventional VO, our networks predict camera pose (tracking) and scene depth (mapping) and simultaneously optimize constraints over the multiple frames (local BA). To realize this purpose, we introduced the depth estimation network, the pose estimation network, and the RNN as a windowed optimizer. Each network architecture is not original, as previously suggested in [8], [9], [10], but our approach is, as far as we know, the first attempt to accomplish tracking, mapping, and optimization simultaneously using an end-to-end deep learning approach.

To enhance our system's robustness, we estimated uncertainty together with the scene depth and the camera pose. Modeling uncertainty allows us to detect inherent errors in the data, such as unusual lighting effects, occlusions, and dynamic objects. In contrast to the previous work in [5], [6], [7] focused on detecting those errors, our method is rooted in

a more general approach of modeling uncertainty suggested by Kendall and Gal [11]. According to them, heteroscedastic aleatoric uncertainty (used in this work) effectively attenuates the residual loss and makes the model robust to noises.

We also benefited from the unsupervised learning scheme. We obtained better-converged models by training with a large-scale unlabeled dataset. Moreover, our system replaced the conventional VO because of the unsupervised training loss. To train our network in an unsupervised manner, we formulated the loss function as a variance-normalized image residual. This is similar to the objective function used in model-based VOs such as [2]. Thus, we achieved the same objective as in the model-based VO, but we imposed the ability to learn the model.

In summary, the proposed method includes:

- a deep neural network for visual tracking, mapping and windowed optimization which can be modularized as in the model-based VO;
- uncertainty modeling to improve estimation performance by carefully rejecting errors and outliers inherent in the data; and
- an unsupervised learning scheme that enables to train the network with unlabeled data.

II. Related Works

In early works, learning-based VOs focused on assisting conventional VO pipelines rather than learning it in an end-to-end fashion. CNN-SLAM [12] utilized depth predictions from the deep networks to determine the absolute scale of the scenes reconstructed from the conventional monocular visual SLAM. Another fascinating work is CodeSLAM [13]. In this work, scene geometry was encoded as a code that originated from the depth auto-encoding networks. Optimization over the code together with conventional SLAM parameters produced better reconstruction performances. DeepTAM [14] suggested mapping and tracking networks jointly working to accomplish localization and mapping within a key-frame. DeepTAM took a step forward as a learning-based VO, but it is difficult to regard it as a fully deep learning approach. As in the conventional method [15], precomputation of photoconsistency cost volume is required to use it as an input for the mapping network.

End-to-end learning-based VO, designed to infer camera poses from the raw input images without adopting conventional VO schemes, has been studied frequently in the recent few years. Most end-to-end learning-based VO focused on predicting relative camera poses using two consecutive image frames from the CNN architectures. DeMoN [16] might be the first attempt at end-to-end learning-based VO using image pairs. In this work, they formulated the egomotion estimation as a supervised learning problem and estimated depth, optical flow, and surface normal simultaneously. A more recent approach to frame-to-frame pose estimation employed unsupervised learning schemes, as in [5], [8], [17], and [10]. Applying monocular depth estimation using left-right image consistency [18], Li et al. proposed UnDeepVO [8], an unsupervised deep learning method for

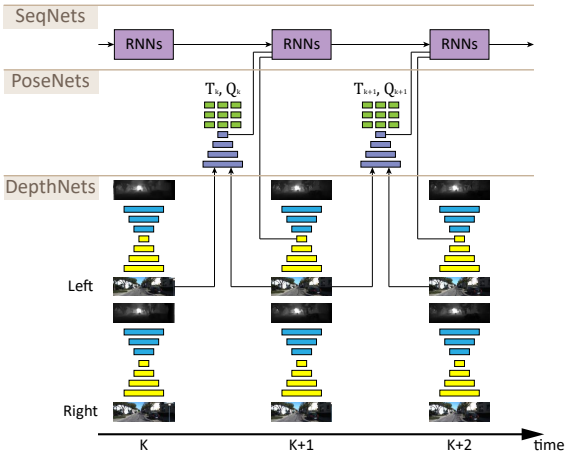

Fig. 2: The proposed deep neural network architecture consists of cascaded depth, pose, and sequential networks.

depth and pose estimation. SfMLearner [5] also proposed depth and pose networks and their networks are trained only with monocular images, unlike UnDeepVO. GeoNet [17] upgraded SfMLearner to handle non-rigid motions in the scene and added geometric consistency loss for the robust ego-motion estimation. Similar attempts to enhance the robustness of learning-based VO appeared in [6], [7] whose main contributions were detecting outlier motions from the scene.

Meanwhile, DeepVO proposed in [9] tackled the ego-motion estimation problem from the SLAM point of view. Rather than inferring poses from the consecutive image pairs, they leveraged RNNs to estimate relative poses while considering sequential dependencies over the whole frame. However, they omitted the mapping process and resided in supervised learning. GANVO [10] is another novel solution to learning-based VO which includes unsupervised learning scheme and RNN architectures. In this method, Generative Adversarial Networks (GANs) generate a depth image and a pose CNN is used to estimate camera poses. At the same time, RNNs propagate features from the pose network so that sequential dependency is considered. Parisotto et al. proposed a more specific approach to reproduce SLAM by using deep learning [19]. Their network consists of local pose estimation, pose selection, and graph optimization modules. However, experiments with only simulated data demonstrated that it is far from the real-world solution.

We proposed an end-to-end learning-based VO using CNN and RNN. Unlike other unsupervised learning-based VOs focused on detecting outliers, we rejected possible errors by modeling uncertainties and incorporating them into the loss functions. Ours also differs from other RNN-based methods in that the pose and the depth are propagated through time. These attributes led to improved estimation results in the experiments.

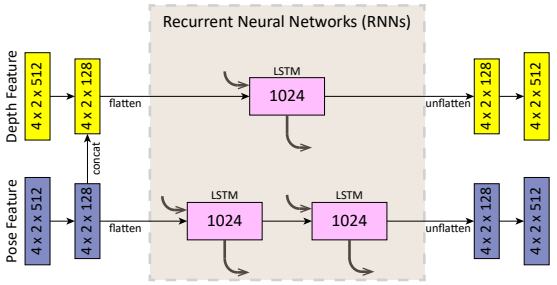

Fig. 3: Detailed structure of the sequential network.

III. Method

A. Network Architecture

Fig. 2 shows the overall network architecture. The network can be divided into three parts; depth, pose, and sequential networks. Note that we separate the pose and depth networks because there is no transfer learning dependency between the two tasks, as proven by [20]. Instead, we use a hierarchy among the networks as delineated in the cascaded architecture. The depth network places at the bottom of the hierarchy because the pose network above it should be trained using the depth predictions. The top sequential network works as a refinement network. This network refines depth and pose by considering the spatiotemporal relationship of the sequential image frames.

We leverage the depth and pose networks from UnDeeoVO [5]. The depth network has a form of autoencoder. This network predicts depth from a single image but learns it by checking consistency between the left and right scenes. The pose network includes CNN layers and fully connected layers. Using this network, we attain relative poses between two consecutive image frames. In addition to depth and pose, we estimate uncertainties to enhance our system's robustness. In the depth network, the decoder part branches into image uncertainty layers and depth uncertainty layers. Likewise in the pose network, image and depth uncertainty layers are attached to the last layer of the CNNs. We also estimate pose uncertainty by branching out the fully connected layers in the pose network.

In the sequential network, we consider dependencies among frames using RNNs. The detailed structure of the sequential network is shown in Fig. 3. It comprises Long Short Term Memory (LSTM)s with 1024 hidden layers. The features in the last layers of the depth encoder and the pose CNN are concatenated and input into the recurrent layers. Thus, we give the depth and pose estimation an opportunity to mutually influence each other, despite initially being trained separately. The encoded features are selectively updated using the previous cell and hidden states. Finally, the learned latent features are again fed into the depth and pose decoders to output the depth and pose predictions optimized over the sequences.

B. Loss Functions

We suggest three types of losses: image consistency, depth consistency, and depth smoothness. Each network is trained individually using different sources of loss computation. For monocular depth estimation, we primarily use spatial consistency (e.g., the consistency between the left and right images) to compute loss. For the pose network, we compute losses using the temporal consistency between the consecutive observations (e.g., the consistency between the k^{th} and $k+1^{\text{th}}$ images). The sequential network's loss is computed from the temporal consistency between non-contagious observations (e.g., the consistency between the k^{th} and $k+2^{\text{th}}$ images).

In addition to depth and pose, our network is designed to estimate uncertainties. Uncertainty estimation captures errors inherent in the data and makes the estimation robust to noise. To include uncertainties in the loss functions, the consistency losses have the form of

$$L_i = \frac{r_i^2}{\sigma_{r_i}^2} + \log \sigma_{r_i}^2, \tag{1}$$

where r_i is the error residual of pixel i in the reference image and $\sigma_{r_i}^2$ is its variance. We will explain how to determine those terms for the image and depth consistency loss respectively, in the following subsections.

1) Image Consistency Loss: The error residual of the image consistency loss is computed from the pixel difference between the reference image I_{ref} and the target image I_{target} when they share common scenes. The error residual is given as

$$r = I_{ref}[\mathbf{x}] - I_{target}[g(\mathbf{x})], \tag{2}$$

where $\mathbf{x} = [u, v]^\top$ indicates a pixel position on the reference image coordinates, and $g(\cdot)$ represents a function that maps a pixel in the reference frame $\mathbf{x}$ to the corresponding pixel in the target image.

Depending on the relation between the two images, there are diverse ways to define the projection function $g(\cdot)$. When the two images are captured from two cameras with a particular spatial relationship, such as from a stereo camera system, the stereo-projection function is given as

$$g(\mathbf{x}_{left}, d_{left}) = \mathbf{x}_{right} = \mathbf{x}_{left} + [Bf/d_{left}, 0]^\top. \tag{3}$$

This means that the corresponding pixel in the right image $\mathbf{x}_{right}$ can be achieved using baseline B, camera focal length f and scene depth d_{left}, assuming that the stereo images are rectified beforehand. When the images are captured at different times from a single camera, the temporal projection function is

$$g(\mathbf{x}_k, d_k, T_k(\xi)) = \mathbf{x}_{k+1} = \pi[T_k(\xi)\pi^{-1}(\mathbf{x}_k, d_k)]. \tag{4}$$

Here, the camera projection function $\pi(\cdot)$ maps 3D point $\mathbf{p}$ to 2D pixel $\mathbf{x}$ as $\mathbf{x} = \pi(\mathbf{p})$. $T_k(\xi)$ is the $SE(3)$ transformation between the k^{th} and $k+1^{\text{th}}$ camera poses and $\xi \in se(3)$ indicates the associated Lie-algebra.

Because the two projection functions are dissimilar (i.e., stereo and temporal), the variances of the spatial and temporal image residuals are also different. The spatial image residual's variance is computed using uncertainty propagation, as

$$\sigma_r^2 = 2\sigma_I^2 + \left(\frac{\partial r}{\partial d_{left}}\right)^2 \sigma_{d_{left}}^2. \tag{5}$$

It consists of the image intensity variance σ_I^2 and the depth variance $\sigma_{d_{left}}^2$ multiplied by the partial derivative of the image residual with respect to the depth $\frac{\partial r}{\partial d_{left}}$. The variance of the temporal image residual is computed simililarly, as

$$\sigma_r^2 = \underbrace{2\sigma_I^2 + \left(\frac{\partial r}{\partial d_k}\right)^2 \sigma_{d_k}^2}_{\text{data-related variance}} + \underbrace{\left(\frac{\partial r}{\partial \xi}\right)\mathbf{Q}\left(\frac{\partial r}{\partial \xi}\right)^\top}_{\text{pose-related variance}}. \tag{6}$$

It includes the covariance of the relative pose $\mathbf{Q}$ because the temporal image residual is dependent on the relative pose.

In practice, we can directly learn residual variances without predicting each component by arranging the image consistency loss in the form of (1) and by computing the error residuals and the variances directly from the networks. For the temporal image variance, however, we need to explicitly learn pose covariance $\mathbf{Q}$ because gauging the pose uncertainty is essential for the SLAM system and for its users. Thus, we divide the variance into two parts: the data-related variance (which includes the first and second terms) and the pose-related variance (the third term). For the ease of nomenclature, we call the data-related variance the image variance. The network outputs the image variances and the pose covariance $\mathbf{Q}$. Then, the pose-related variances are computed by numerically calculating the partial derivative $\partial r/\partial \xi$ and multiplied by the pose covariance $\mathbf{Q}$.

Fig. 4 illustrates the source (k^{th}) and the target ($k+1^{\text{th}}$) scenes and their temporal image variances overlaid with the target scenes. The image variances successfully capture inherent errors in the scene caused by unusual lighting, occlusions, and moving objects. Thus, the loss computed from the pixels with inherent errors is mitigated. This results in robust estimation in negligence of those errors.

2) Depth Consistency Loss: The error residual of depth consistency loss is computed from the depth difference between the reference depth image D_{ref} and the target depth image D_{target}. The error residual is given as

$$r = D_{ref}[\mathbf{x}] - D_{target}[g(\mathbf{x})], \tag{7}$$

where $g(\cdot)$ is the projection function proposed in (3) and (4).

The variance of the depth error residual is also given for the spatial and temporal residuals, respectively. The variance of the spatial depth residual is given as

$$\sigma_r^2 = \left(\frac{\partial r}{\partial d_{left}}\right)^2 \sigma_{d_{left}}^2 + \left(\frac{\partial r}{\partial d_{right}}\right)^2 \sigma_{d_{right}}^2, \tag{8}$$

and it is composed of the residual's partial derivatives with respect to the depth from the left and right images and each

(a) Unusual lightings

(b) Occlusions

(c) Moving objects

Fig. 4: Sample scenes and the estimated image variances. The images in the left column are source images and the images in the right column are target images overlaid with the image variances. The pixel is color-coded by the image variance value showing red color for a larger variance. The sample scenes are classified into three categories based on the cause of inherent errors in the scene.

depth variance. The variance of the temporal depth residual contains the pose-related variance. It is given as

$$\sigma_r^2 = \underbrace{\left(\frac{\partial r}{\partial d_k}\right)^2 \sigma_{d_k}^2 + \left(\frac{\partial r}{\partial d_{k+1}}\right)^2 \sigma_{d_{k+1}}^2}_{\text{data-related variance}} + \underbrace{\left(\frac{\partial r}{\partial \xi}\right)\mathbf{Q}\left(\frac{\partial r}{\partial \xi}\right)^\top}_{\text{pose-related variance}}. \tag{9}$$

Similar to the image consistency loss, the data-related variance in the depth consistency loss is called the depth variance and is directly estimated from the network. The pose-related variance is also computed in a similar way using the partial derivative $\partial r/\partial \xi$ and the pose covariance $\mathbf{Q}$.

3) Depth Smoothness Loss: Depth smoothness loss smooths out the estimated depth in the pixels with little intensity differences between neighboring pixels.

$$L = |D_u| \exp(-|I_u|) + |D_v| \exp(-|I_v|), \tag{10}$$

where D_u and D_v are depth gradients and I_u and I_v are image gradients with respect to u and v directions.

C. Training Procedure

The entire network should be learned sequentially to benefit from the hierarchy depicted in Fig. 2. The depth

network, which outputs the scene depth, is trained first. Training the depth network in an unsupervised manner is particularly difficult because the monocular input image gives little information about the scene depth. Thus, we use the stereo images where the larger pixel disparity between correspondences implies smaller depth values. As a result, we compute the loss by checking the consistency between the left and right images as

$$L_{DN} = \sum_{j=1}^{l} \sum_{i=1}^{n} L_{i,j}^{Image} + L_{i,j}^{Depth} + L_{i,j}^{Smoothness}, \quad (11)$$

where L^{Image}, L^{Depth} and $L^{Smoothness}$ are the image consistency loss from (1) and (2), the depth consistency loss from (1) and (7), and the smoothness loss from (11) in the previous section. Because we use images with l resolutions, the loss is summed over every i^{th} pixel and every j^{th} image pyramid. Even though we use stereo images for the training, depth is predicted from the single image at the inference phase.

The pose network is then trained by checking the consistency between temporally adjacent images. Because depth is given in the previously trained depth network, finding dense correspondences between the sequential images comes in handy so as to compute the consistency losses. The overall loss for training the pose network includes image and depth consistency losses, given as

$$L_{PN} = \sum_{j=1}^{l} \sum_{i=1}^{n} L_{i,j}^{Image} + L_{i,j}^{Depth}. \quad (12)$$

In this training phase, we freeze the depth network's parameters and train only the pose network. Otherwise, the depth estimation accuracy would be degraded significantly because of the depth inconsistency originating from moving objects.

We train the sequential network after training the depth and pose networks. After fixing other layers, only latent depth and pose features are passed into the RNNs and learned again to refine the depth and pose predictions. We use the temporal consistency losses and the smoothness loss to train the sequential network. The loss is given as

$$L_{SN} = \sum_{k=1}^{m} \sum_{j=1}^{l} \sum_{i=1}^{n} L_{i,j,k}^{Image} + L_{i,j,k}^{Depth} + L_{i,j,k}^{Smoothness}. \quad (13)$$

The losses from m image pairs within a time window are summed over to train the RNNs via truncated Backpropagation Through Time (BPTT). The temporally contagious and non-contagious image pairs are used to compute the loss.

IV. Experiment

We conducted experiments on publicly available outdoor and indoor datasets. We used the KITTI odometry dataset [21] for the outdoor experiment and EuRoC MAV dataset [22] for the indoor experiment. Since the possible ranges of pose and depth values are dissimilar, we needed to train the networks separately for the outdoor and indoor scenes. In each experiment, we demonstrated the pose and depth estimation results.

A. Training Details

The proposed architecture was implemented using Tensorflow and trained with NVIDIA Geforce GTX 1080 Ti. We used an Adam optimizer [23] with $\beta_1 = 0.9$, $\beta_2 = 0.999$, and an initial learning rate of 10^{-4}. The learning rate was gradually decreased by a half and a quarter of the initial value at the $3/5$ and $4/5$ of the total iterations. Each network was trained individually. First, we trained the depth network for 60 epochs with a batch size of 16. Then, we trained the pose network using the same number of epochs and the same batch size. Finally, we trained the sequential network for 20 epochs with a batch of five consecutive images. We resized the input image into a resolution of 256×512 and generated four additional levels of image pyramids. When training the depth and pose networks, we augmented the input data by randomly selecting half of the images and shifting their gamma, brightness, and color values. When training a sequential network, we skipped this process to keep consistency among consecutive input images.

B. KITTI Odometry Dataset Experiment

The KITTI odometry dataset [21] is the most widely used odometry benchmark dataset, and it includes stereo images, LiDAR data, and ground truth poses estimated from the GPS and IMU. Pose and depth evaluations are readily available via ground truth poses and depths acquired from the LiDAR points. Similar to other learning-based VOs like in [5], [8], we used sequence `00-08` as a training set and `09-10` as a testing set. We used stereo images for the training, but we only used the left camera images in the test phase.

1) Pose Estimation Evaluation: We adopted average translational and rotational RMSE drifts on the trajectory length of $(100, \cdots, 800)$ meters as the pose evaluation metric. The result appears in Table. I. For comparison, we

TABLE I: Pose estimation results on KITTI dataset

seq	Ours		SfMLearner [5]		UnDeepVO [8]		ORB-SLAM2 [3]	
	t_{rel}	r_{rel}	t_{rel}	r_{rel}	t_{rel}	r_{rel}	t_{rel}	r_{rel}
00	10.80	3.70	66.35	6.13	4.41	1.92	0.7	0.25
01	56.36	2.60	35.17	2.74	69.07	1.60	1.39	0.21
02	11.74	3.40	58.75	3.58	5.58	2.44	0.76	0.23
03	15.27	5.50	10.78	3.92	5.00	6.17	0.71	0.28
04	6.13	3.56	4.49	5.24	4.49	2.13	0.48	0.13
05	8.06	3.08	18.67	4.10	3.40	1.50	0.4	0.16
06	8.42	3.29	25.88	4.80	6.20	1.98	0.51	0.15
07	9.42	5.82	21.33	6.65	3.15	2.48	0.50	0.28
08	12.06	3.51	21.90	2.91	4.08	1.79	1.05	0.32
09	10.36	4.82	18.77	3.21	7.01	3.61	0.87	0.27
10	26.03	7.61	14.33	3.30	10.63	4.65	0.60	0.27
avg	15.88	4.26	26.95	4.24	11.18	2.75	0.72	0.22

t_{rel}: average translational RMSE drift (%) on length of $100\text{m} - 800\text{m}$. r_{rel}: average rotational RMSE drift ($^\circ/100\text{m}$) on length of $100\text{m} - 800\text{m}$. The numbers from others were referenced from [7].

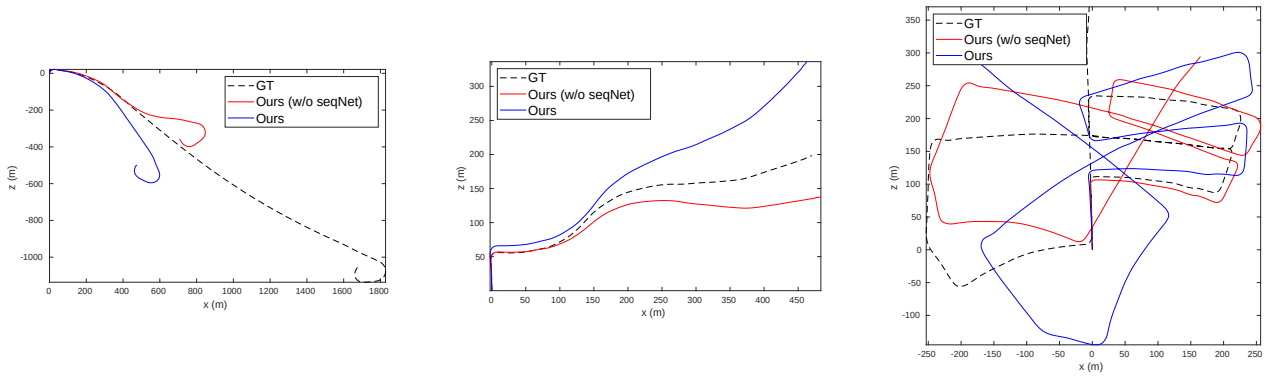

(a) 01 (b) 03 (c) 05

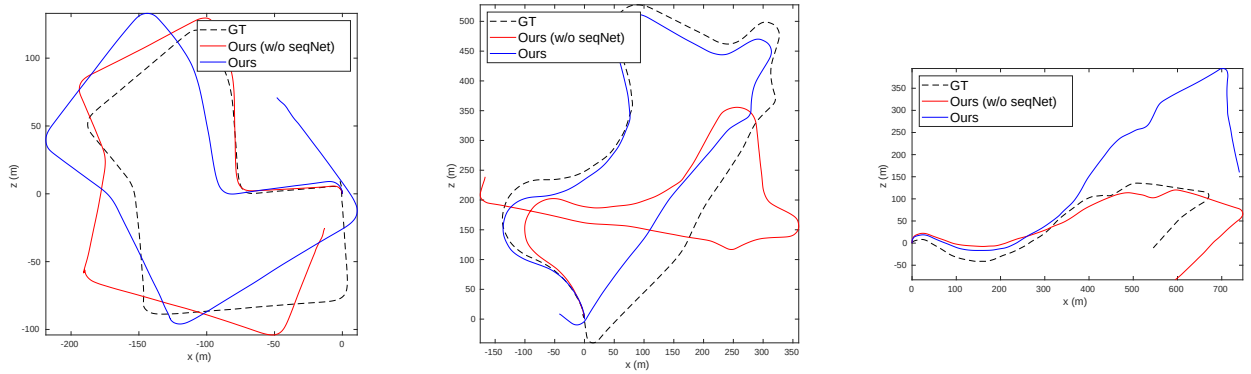

(d) 07 (e) 09 (f) 10

Fig. 5: Estimated trajectories on KITTI odometry dataset. (a) to (d) show validation results while (e) and (f) represent test results. The black dotted lines are the ground truth trajectories while the blue solid lines indicates the estimated trajectories. The red solid lines are estimated from the proposed method without using the sequential network.

TABLE II: Depth estimation results

	Abs Rel	Sq Rel	RMSE	RMSE log	$\delta < 1.25$	$\delta < 1.25^2$	$\delta < 1.25^3$
Ours (KITTI `09`)	0.154	1.008	4.536	0.242	0.772	0.917	0.969
Ours (KITTI `10`)	0.209	1.218	4.288	0.275	0.700	0.888	0.959
Ours (w/o seqNet)	0.177	1.342	5.035	0.276	0.741	0.891	0.953
Ours (w/ seqNet)	**0.169**	**1.185**	**4.901**	**0.264**	0.752	0.895	0.954
SfMLearner [5]	0.201	1.391	5.181	0.264	0.696	0.900	0.966
UnDeepVO [8]	0.183	1.73	6.57	0.268	-	-	-
Monodepth [18]	**0.140**	**0.976**	**4.471**	**0.232**	0.818	0.931	0.969

All the results were computed using the depth capped at 50m. We present our result on the KITTI odometry test set (sequence `09` and `10`) as in the first and the second rows and on the KITTI test set proposed by Eigen et al [24] as in the third and fourth rows. Note that our model and UnDeepVO[8] was trained using KITTI odometry dataset while other methods were trained using the full KITTI dataset. The result from others are the numbers reported from their works as it is.

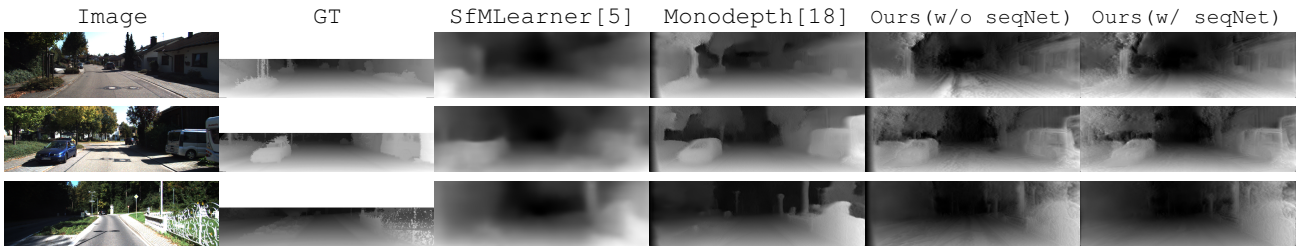

Fig. 6: Depth prediction results selected from the KITTI odometry `09` sequence. To better illustrate, we present disparity maps instead of depth maps. The results of other methods were obtained by using the codes and learned models provided by the authors.

provided results from other unsupervised learning-based VOs [5] and [8] and from a model-based approach [3].

On average, ours shows comparable performance with other learning-based approaches. UnDeepVO outperforms in most sequences except in `01`, which includes highway scenes. Given that the translational drift of the well-optimized model-based approach, such as ORB-SLAM2, in sequence `01` is double of its average drift, UnDeepVO's error degradation on the highway sequence is remarkable. However, ours shows improved performance in this sequence. This implies that ours can be used more generally in a variety of environments with moderate performance. We suppose that the generality results from the proposed uncertainty modeling and sequential training.

Fig. 5 shows the predicted camera trajectories against the ground truth trajectories. Overall, the estimated trajectories are consistent with the ground truth trajectories. We also provide results without using the sequential network. We can detect improvements after applying the sequential network, especially in rotational drifts of test sequences.

2) Depth Estimation Evaluation: Table. II shows the depth evaluation results. Our depth was evaluated with Eigen's test split [24]. We compared the result with other methods evaluated using the same error metrics. Ours performs better than other learning-based VO approaches and slightly worse than Monodepth [18], which focuses only on the monocular depth estimation. For an ablation study, the result from not using the sequential network is given in the third row. The improved performance certifies that the sequential network further refines depths by considering dependencies over multiple frames. We also evaluated the depth estimation performance of the KITTI odometry test sets, as shown in the first and second rows. Our method is designed for the depth estimation of sequentially related scenes, so these results demonstrate more general performance and could be compared with other methods in the future.

Fig. 6 illustrates sample scenes and their estimated depth from KITTI odometry sequence `09`. Our depth shows qualitative improvement over that of SfMLearner [5]. Monodepth [8] shows better performance especially in the farther depth, but our result with a sequential network is comparable. In near depth, details such as tree branches are captured well through our predictions.

C. EuRoC Dataset Experiment

The EuRoC MAV dataset [21] contains stereo images and inertial sensor data collected from a mobile aerial vehicle (MAV). It also provides sensor calibration information and ground truth vehicle poses estimated from a motion capture system and from a laser tracker. Data was collected in three indoor environments: `Machine Hall`, `Vicon Room 1`, and `Vicon Room 2`. The vehicle's motion varies, and the data were categorized according to the complexity of the motions. We used the `Machine Hall 05` dataset, which contains highly dynamic motions, for the test and the remaining datasets for the training.

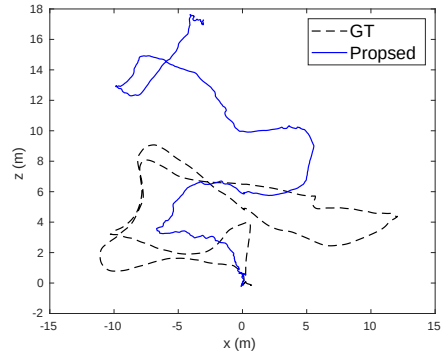

(a)

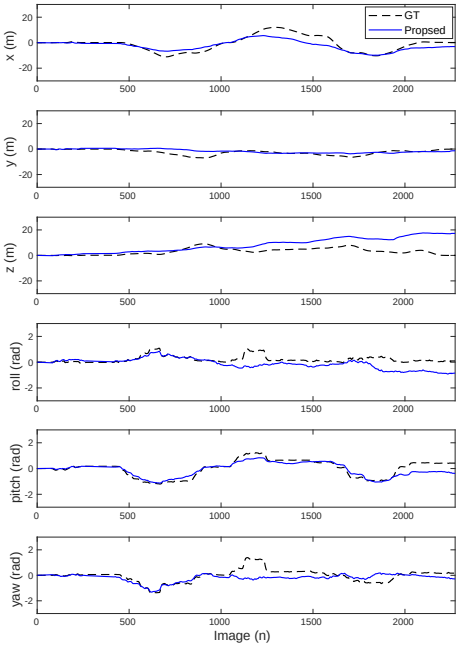

(b)

Fig. 7: The estimated camera poses from `Machine Hall 05` of the EuRoC dataset. (a) shows the estimated trajectory against the ground truth trajectory. (b) illustrates the estimated positions and rotations in each axis.

1) Pose Estimation Evaluation: Fig. 7 depicts the estimated trajectory and the positions and rotations in each axis. Our system recognized relatively simple motions such as taking off, but it sometimes failed to capture complex motions such as abrupt changes in roll, pitch, and yaw angles near the 1100^{th} image frame. We need more abundant data to capture intricate motions. We used over 20,000 training images, similar to the amount of data we used to train the outdoor car motions, but this is still limited because a MAV's motion is more complicated than that of cars.

2) Depth Estimation Evaluation: The ground truth depth is missing in the provided dataset, so only the qualitative evaluation is available, as shown in Fig. 8. To examine the

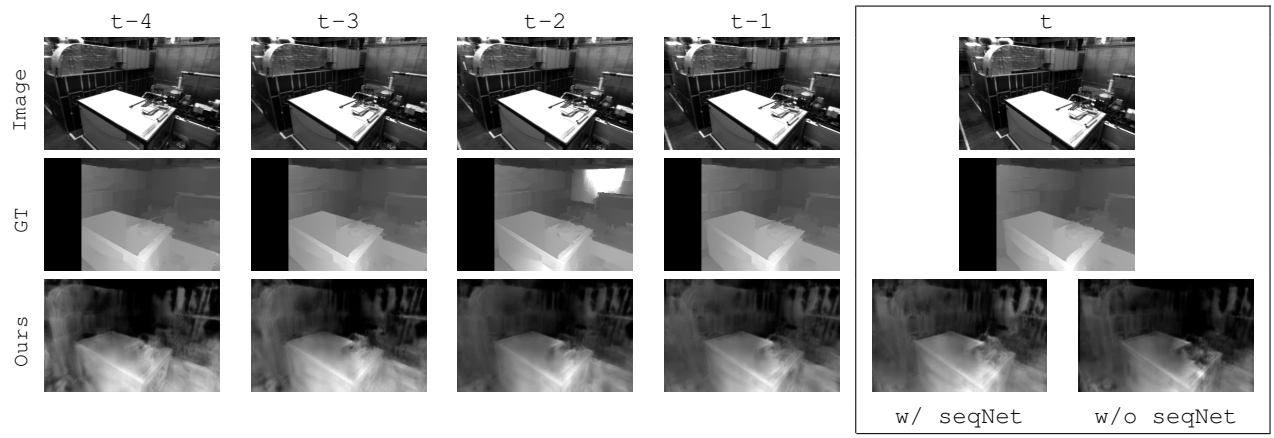

Fig. 8: Sample depth predictions from `Machine Hall 05` of the EuRoC dataset. Sequential input images at times $(t-4, \cdots, t)$ are in the first row. The corresponding depths estimated from stereo matching and our networks are shown in the second and thrid rows. At time t, we present our estimated depth with and without using the sequential network.

validity of our prediction, the reference depth images are generated with a stereo-matching algorithm [25] and presented in the second row of this figure. The proposed approach presents a similar tendency with the reference depth where near objects and distant walls are distinguished by depth. Moreover, we demonstrate the sequential network's effect by showing depth predictions within a temporal window of size five. Depth prediction evolves as the system observes more scenes. Compared to the depth estimated from a single scene, the depth from multiple scenes preserves more details.

V. Conclusions

We proposed an unsupervised learning based VO using CNN and RNN architectures. We suggested loss functions mitigated by uncertainties to learn the model. In the inference phase, the tracking (pose estimation) and the mapping (depth estimation) were accomplished in an end-to-end manner. The experiments with indoor and outdoor datasets demonstrated our method's promising performance with respect to pose and depth estimation in various environments. For future work, the proposed method can be adopted as a front-end of the full SLAM system.

References

[1] C. Forster, M. Pizzoli, and D. Scaramuzza, "SVO: Fast semi-direct monocular visual odometry," 2014, pp. 15–22.

[2] J. Engel, T. Schöps, and D. Cremers, "LSD-SLAM: Large-scale direct monocular slam." Springer, 2014, pp. 834–849.

[3] R. Mur-Artal and J. D. Tardós, "ORB-SLAM2: An open-source slam system for monocular, stereo, and RGB-D cameras," vol. 33, no. 5, pp. 1255–1262, 2017.

[4] J. Engel, V. Koltun, and D. Cremers, "Direct sparse odometry," *IEEE transactions on pattern analysis and machine intelligence*, vol. 40, no. 3, pp. 611–625, 2018.

[5] T. Zhou, M. Brown, N. Snavely, and D. G. Lowe, "Unsupervised learning of depth and ego-motion from video," 2017, pp. 1851–1858.

[6] C. Luo, Z. Yang, P. Wang, Y. Wang, W. Xu, R. Nevatia, and A. Yuille, "Every pixel counts++: Joint learning of geometry and motion with 3D holistic understanding," *arXiv preprint arXiv:1810.06125*, 2018.

[7] A. Z. Zhu, W. Liu, Z. Wang, V. Kumar, and K. Daniilidis, "Robustness meets deep learning: An end-to-end hybrid pipeline for unsupervised learning of egomotion," *arXiv preprint arXiv:1812.08351*, 2018.

[8] R. Li, S. Wang, Z. Long, and D. Gu, "UnDeepVO: Monocular visual odometry through unsupervised deep learning," 2018, pp. 7286–7291.

[9] S. Wang, R. Clark, H. Wen, and N. Trigoni, "End-to-end, sequence-to-sequence probabilistic visual odometry through deep neural networks," vol. 37, no. 4-5, pp. 513–542, 2018.

[10] Y. Almalioglu, M. R. U. Saputra, P. P. de Gusmao, A. Markham, and N. Trigoni, "GANVO: Unsupervised deep monocular visual odometry and depth estimation with generative adversarial networks," *arXiv preprint arXiv:1809.05786*, 2018.

[11] A. Kendall and Y. Gal, "What uncertainties do we need in bayesian deep learning for computer vision?" in *Advances in neural information processing systems*, 2017, pp. 5574–5584.

[12] K. Tateno, F. Tombari, I. Laina, and N. Navab, "CNN-SLAM: Real-time dense monocular SLAM with learned depth prediction," 2017, pp. 6243–6252.

[13] M. Bloesch, J. Czarnowski, R. Clark, S. Leutenegger, and A. J. Davison, "CodeSLAM-learning a compact, optimisable representation for dense visual SLAM," *arXiv preprint arXiv:1804.00874*, 2018.

[14] H. Zhou, B. Ummenhofer, and T. Brox, "DeepTAM: Deep tracking and mapping," 2018.

[15] R. A. Newcombe, S. J. Lovegrove, and A. J. Davison, "DTAM: Dense tracking and mapping in real-time." IEEE, 2011, pp. 2320–2327.

[16] B. Ummenhofer, H. Zhou, J. Uhrig, N. Mayer, E. Ilg, A. Dosovitskiy, and T. Brox, "DeMoN: Depth and motion network for learning monocular stereo," 2017, pp. 5038–5047.

[17] Z. Yin and J. Shi, "GeoNet: Unsupervised learning of dense depth, optical flow and camera pose," 2018, pp. 1983–1992.

[18] C. Godard, O. Mac Aodha, and G. J. Brostow, "Unsupervised monocular depth estimation with left-right consistency," 2017, pp. 270–279.

[19] E. Parisotto, D. S. Chaplot, J. Zhang, and R. Salakhutdinov, "Global pose estimation with an attention-based recurrent network," *arXiv preprint arXiv:1802.06857*, 2018.

[20] A. R. Zamir, A. Sax, W. Shen, L. J. Guibas, J. Malik, and S. Savarese, "Taskonomy: Disentangling task transfer learning," 2018, pp. 3712–3722.

[21] A. Geiger, P. Lenz, and R. Urtasun, "Are we ready for autonomous driving? the KITTI vision benchmark suite," 2012, pp. 3354–3361.

[22] M. Burri, J. Nikolic, P. Gohl, T. Schneider, J. Rehder, S. Omari, M. W. Achtelik, and R. Siegwart, "The EuRoC micro aerial vehicle datasets," vol. 35, no. 10, pp. 1157–1163, 2016.

[23] D. P. Kingma and J. Ba, "Adam: A method for stochastic optimization," *arXiv preprint arXiv:1412.6980*, 2014.

[24] D. Eigen, C. Puhrsch, and R. Fergus, "Depth map prediction from a single image using a multi-scale deep network," in *Advances in neural information processing systems*, 2014, pp. 2366–2374.

[25] H. Hirschmuller, "Accurate and efficient stereo processing by semi-global matching and mutual information," vol. 30, no. 2, pp. 328–341, 2008.